Nuclear Instruments and Methods in Physics Research A 595 (2008) 353–358

Contents lists available at ScienceDirect

Nuclear Instruments and Methods in Physics Research A

journal homepage: www.elsevier.com/locate/nima

Experimental demonstration of a hybrid photon detector concept based on the Timepix detector

Tilman K. Rügheimer [a,*], Ulrike Gebert [a], Thilo Michel [a], Gisela Anton [a], Jacques Séguinot [b], Christian Joram [b]

[a] Erlangen Centre for Astroparticle Physics, Universität Erlangen-Nürnberg, Erwin-Rommel-Str. 1, 91058 Erlangen, Germany
[b] CERN PH, Geneva, Switzerland

ARTICLE INFO

Article history:
Received 13 April 2008
Received in revised form
11 July 2008
Accepted 13 July 2008
Available online 19 July 2008

Keywords:
Photo-detection
Hybrid photon detector
HPD
Timepix
Medipix

ABSTRACT

Hybrid photon detectors with pixelated readout electronics allow for photo-detection with a high spatial resolution. We present the concept of a hybrid photon detector based on the 65k-pixel detector "Timepix". First experiments of the Timepix detector with photo-electrons were carried out and demonstrate that the concept combines good spatial and time resolutions for photo-electron detection. By comparison of the experimental data with GEANT4 simulations we identify the limiting factors for the time resolution: Electron backscattering from the sensor surface and charge-sharing among neighboring pixels in combination with the finite rise time of the preamplifier output pulse. Levers for its improvement in a future dedicated detector design are identified.

1. Introduction

Photo-detection is a key technology in a wide field of investigations ranging from relatively small-scale optical spectroscopy experiments in chemistry, atomic and solid-state physics [1–3] up to large Cherenkov telescopes such as the neutrino telescopes ANTARES/KM3NeT [4,5] or IceCube [6] equipped with thousands of photo-multipliers. Excellent single-photon resolution, high-rate performance, and high time resolution are typical experimental requirements that photo-detectors have to fulfill.

With the advent of highly sophisticated pixelated semiconductor detectors spatial resolution has also become an important criterion since detectors with a high number of parallel channels can be designed. The mass-production of several hundred hybrid photon detectors (HPDs) for the two Ring Imaging Cherenkov (RICH) counters of the LHCb experiment at CERN has proven the technical feasibility of the hybrid concept. It uses a semiconductor anode for the detection of photo-electrons that are released from a photo-cathode irradiated by photons [7,8].

In this paper we present the concept of an HPD based on the Timepix detector [9] that was developed within the Medipix collaboration [11]. Continuous data acquisition, high spatial resolution provided by a high number of independent pixels, single-photon resolution, high time resolution, and the capability of application-specific on-chip data processing and reduction are key advantages of our concept [12].

2. Concept of an HPD based on the Timepix detector

2.1. The Timepix detector of the Medipix family

Detectors of the Medipix family are flip-chip pixel detectors [11,13]. They consist of a semiconductor sensor layer and a pixelated electronics layer ASIC which are electrically connected to each other in each pixel using the bump bond technique. The assembly is made up of 256×256 square pixels with a pixel pitch of 55 μm. Each pixel electronic circuit contains a charge-sensitive preamplifier, a discriminator, and a counter. The system enables the counting of single electrons or other particles which have deposited an energy above the adjustable discriminator threshold.

The Timepix detector [9] is a further development of the Medipix detector. It operates with a clock adjustable up to 100 MHz which is used for two additional operation modes: the Timepix mode and the Time-Over-Threshold mode (TOT mode). In the Timepix mode the counting of clock pulses is started when a signal exceeds the discriminator threshold and is stopped at the end of the acquisition frame. It thus performs the determination of the detection time of an event with a precision inverse of the clock frequency. In the TOT mode the clock pulses are counted as long as the signal is above threshold. This can be used to obtain the energy deposition in a pixel.

* Corresponding author.
E-mail address: tilman.ruegheimer@physik.uni-erlangen.de (T.K. Rügheimer).

0168-9002/$ - see front matter © 2008 Elsevier B.V. All rights reserved.
doi:10.1016/j.nima.2008.07.079

2.2. The concept of a continuously operating HPD

The HPD concept consists of a sealed vacuum tube with a photo-cathode at the top, a Silicon anode at the bottom, and an electric field in between. Spatial resolution is achieved by the use of a pixelated anode, e.g., the Timepix detector with a pixel pitch of 55 μm (cf. Fig. 1). An appropriate cross-focussing electric field configuration reduces the time dispersion of photo-electrons arriving at the sensor to the sub-nanosecond scale and the size of the point spread function amounts to a few pixels only. The imaging properties of an HPD are then determined predominantly by the response of the pixelated Silicon detector to an incident photo-electron.

The LHCb experiment uses external triggering to determine the event time. The underlying pixel detector, however, could also be used for self-triggered read-out. Our Timepix-based concept aims at the design of a continuously operating HPD that determines the event time without any external trigger signal using an integrated clock and delivers fully digitized data through the electronics integrated in every single pixel.

At the moment, continuous data acquisition is not yet possible with the Timepix detector. The serialized matrix readout provided by the currently used chip readout board introduces a dead-time of about 9 ms during which impinging photo-electrons cannot be detected. A future generation of the chip, however, could be instrumented with two independent counters operating alternately and read out using a parallel interface to overcome this issue. In this way continuous and dead-time free data acquisition without an external trigger can be achieved which makes such an HPD ideally suited for experiments requiring an absolute timing information without an external trigger signal, e.g., in astroparticle or medical physics.

3. Experimental detection of photo-electrons with the Timepix detector

3.1. The HPD test set-up

We investigated the response of the Timepix detector to photo-electrons, i.e., electrons released from a photo-cathode in vacuum due to an incident light pulse. For this purpose the detector was incorporated into a pumped vacuum test set-up that was operated at a base pressure of about 5×10^{-6} hPa. Photo-electrons were released from a CsI photo-cathode exposed to light pulses from a self-triggering UV discharge lamp with a pulse duration of less than 3 ns. The photo-electrons were accelerated towards the detector in a proximity-focussed electron optics (cf. Fig. 2). Several values between 6 and 20 keV were chosen for the electric potential difference ΔV between the photo-cathode and the detector (cf. Ref. [14] for more details on the set-up). The "MUROS" readout [15] and the software package "Pixelman" [16] were used for the data acquisition.

Due to the random occurrence of lamp pulses an indirect determination of the event time was necessary. For this purpose we operated the detector in the Timepix mode and used standard analog delay electronics to complete the acquisition frame at a fixed time interval of 3.00 μs after the lamp signal. Throughout this paper, we define the time origin to be the end of the acquisition frame. The detection time of a photo-electron signal is relative to this origin.

3.2. Event time determination and resolution

Fig. 3a (solid curve) shows a histogram over all pixels of the detector and 50,000 frames recorded for an electric potential difference between photo-cathode and detector of 20 keV and a discriminator threshold of 4.7 keV. The energy calibration of the discriminator threshold was carried out using fluorescence radiation and radioactive sources. A clear but asymmetric peak arises at −3060 ns. It is attributed to photo-electrons released from the photo-cathode by flashes from the discharge lamp. This clearly shows that the Timepix detector can be used in an HPD for time-resolved photo-electron detection.

The dark-count rate can be determined from the constant count-rate at times before and after the peak yielding a value of 83.25 kHz/cm^2 at 20 keV. These counts are due to spontaneous thermal emission of electrons from the photo-cathode. Our experience with the given set-up shows that the high dark-count rate is the price one has to pay when using a CsI photo-cathode. However, for experimental reasons CsI is the material of choice at the current stage of our experiments since it survives exposition to air on the time-scale of 30 min and thereby facilitates the assembly of the HPD test set-up.

The time resolution, however, suffers from electron backscattering from the sensor surface [17] and from charge-sharing among neighboring pixels, the latter being a well-known phenomenon occurring for detectors with rather small pixels [18]. This is seen in

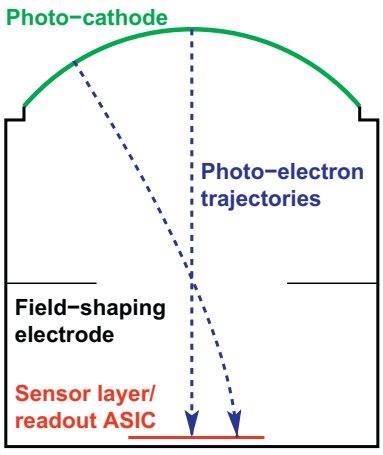

Fig. 1. (Color online) Schematic drawing of the HPD concept with photo-cathode, field-shaping electrode, sensor layer, and readout ASIC. Two exemplary photo-electron trajectories are drawn to illustrate the cross-focussing optics.

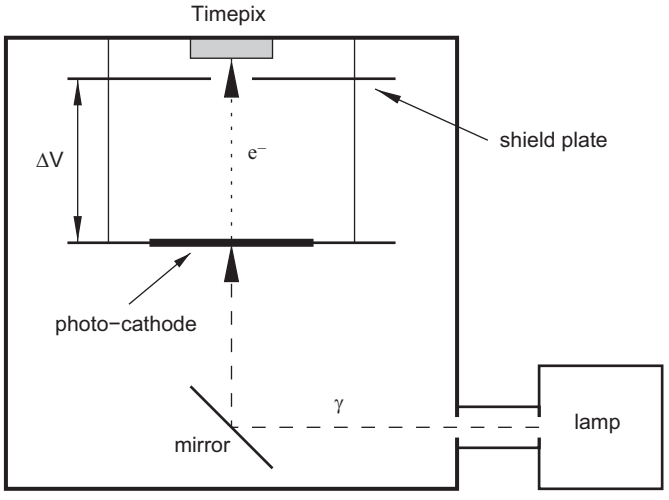

Fig. 2. Schematic drawing of the HPD test set-up with the Timepix detector mounted upside-down. The distance between the photo-cathode and the sensor surface is 41 mm and the electric potential difference ΔV can be set to values up to 20 kV. The shield plate has a small opening of 15 mm diameter.

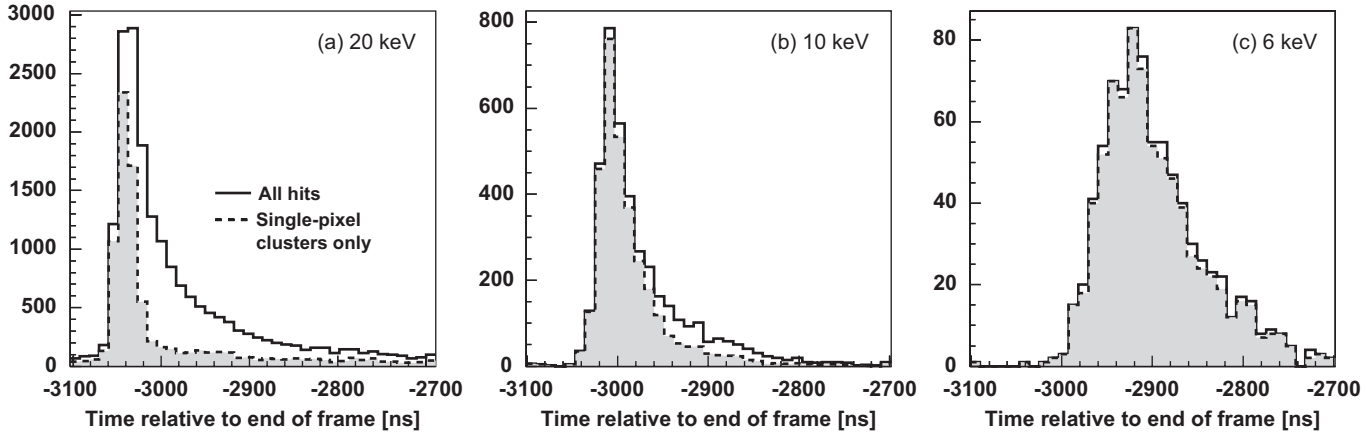

Fig. 3. Measured event time distribution relative to the end of the acquisition frame for photo-electron energies of (a) 20 keV, (b) 10 keV, and (c) 6 keV. The origin of the time axis corresponds to the end of the frame. The peak is attributed to photo-electrons that are emitted from the photo-cathode by pulses from the discharge lamp. The solid curves contain all hits, whereas the dashed curves refer to single-pixel clusters only.

the experimental data if only single-pixel clusters are considered for the histogram (dashed curve in Fig. 3a). Leaving out larger clusters requires that the energy deposition in each adjacent pixel be below the energy threshold of 4.7 keV thereby suppressing charge-sharing in the data. A Gaussian fit of the dashed curve yields a width of 10.5 ns (sigma) which agrees with the expectations when operating the detector clock at 100 MHz.

Understanding the influence of backscattering and charge-sharing on the time resolution still requires the knowledge of the shape and the duration of the amplified charge pulse at the input of the discriminator, more precisely of its rising edge. The design of the pixel electronics is such that the height of the preamplifier output pulse is directly proportional to the energy deposition. The peaking time, however, is constant regardless of the energy deposition and can be adjusted in the range of 90–180 ns [9,10]. Consequently, the lower the energy deposition the later the discriminator threshold is exceeded. Figs. 3b–c illustrate this time walk for the same energy threshold but photo-electron energies of 10 and 6 keV, respectively. We will refer to this aspect in Section 4.3 when discussing the data in the context of Monte Carlo simulations of the detector response.

3.3. Spatial distribution

While the data were integrated over all pixels to yield the time distribution in Fig. 3, image plots of the data in Figs. 4a and b show the spatial distribution of the photo-electron hits. An integration along rows and columns was performed, respectively, in order to obtain sufficiently high statistics. The sensor area exposed to "true" photo-electrons, i.e., photo-electrons released by a flash from the UV lamp, is rather large due to the size of the beam spot. The set-up therefore does not allow for the determination of the spatial resolution inherent to the detector. In an HPD prototype the electron optics design would be cross-focussing leading to a very good spatial resolution.

4. Simulation of the detector response and comparison with the experimental data

4.1. Overview of the GEANT4 simulation

Understanding the duration of the photo-electron peak and in particular its asymmetry towards later detection times (cf. Figs. 3a–c) requires a detailed investigation of the energy deposition of the photo-electrons in the sensor layer and the signal generation process in the pixel electronics. We simulated the detector energy response function and combined these results with a model for the shape of the preamplifier output pulse to reproduce the experimental data. From further simulations the time-spread of the secondary charges arriving at the pixel electrodes is known to be less than 1 ns (sigma) and therefore does not need to be taken into account [19].

Monte Carlo simulations of the detector response were carried out using the GEANT4 simulation framework [20,21]. A region of 3×3 pixels was homogeneously illuminated with electrons of primary energy 20 keV and the energy deposition in the central pixel was analyzed.

The energy loss of the photo-electron in the sensor originates from scattering with atomic shell electrons, and to a very small degree from radiative losses (Bremsstrahlung). This includes electron backscattering from the surface [17]. The GEANT4 low-energy parametrizations of the interaction cross-sections were used [22].

The energy deposition due to continuous losses was converted into a number of electron–hole pairs for each propagation step assuming a production energy of 3.6 eV per pair in silicon. Due to the doping of the sensor only holes are collected at the pixel electronics.

The lateral diffusion of the charge cloud in the sensor during the drift to the pixel electrodes was modeled by projecting each charge onto the detector pixel matrix using independent Gaussian distributions of equal width for both lateral directions. The Gaussian width depends on the sensor bias voltage (150 V), the sensor thickness (300 μm), and the Coulomb repulsion between the generated charges. It was modeled as described earlier in the literature [18,23] and amounts to 7.8 μm (sigma). The importance of the charge-sharing effect is evident when comparing this value with the pixel pitch of 55 μm.

4.2. The Timepix energy response function

Fig. 5 shows the energy response function on a logarithmic scale as obtained from the simulation described above. The peak at 19.2 keV (cf. inset in Fig. 5 for a plot on linear scale) corresponds to the deposition of the total photo-electron energy in one pixel and appears below the primary energy of 20 keV due to losses in the highly doped n^{++}-layer at the top of the sensor. A thickness of 200 nm was assumed for this dead layer which is in the range specified by the manufacturer.

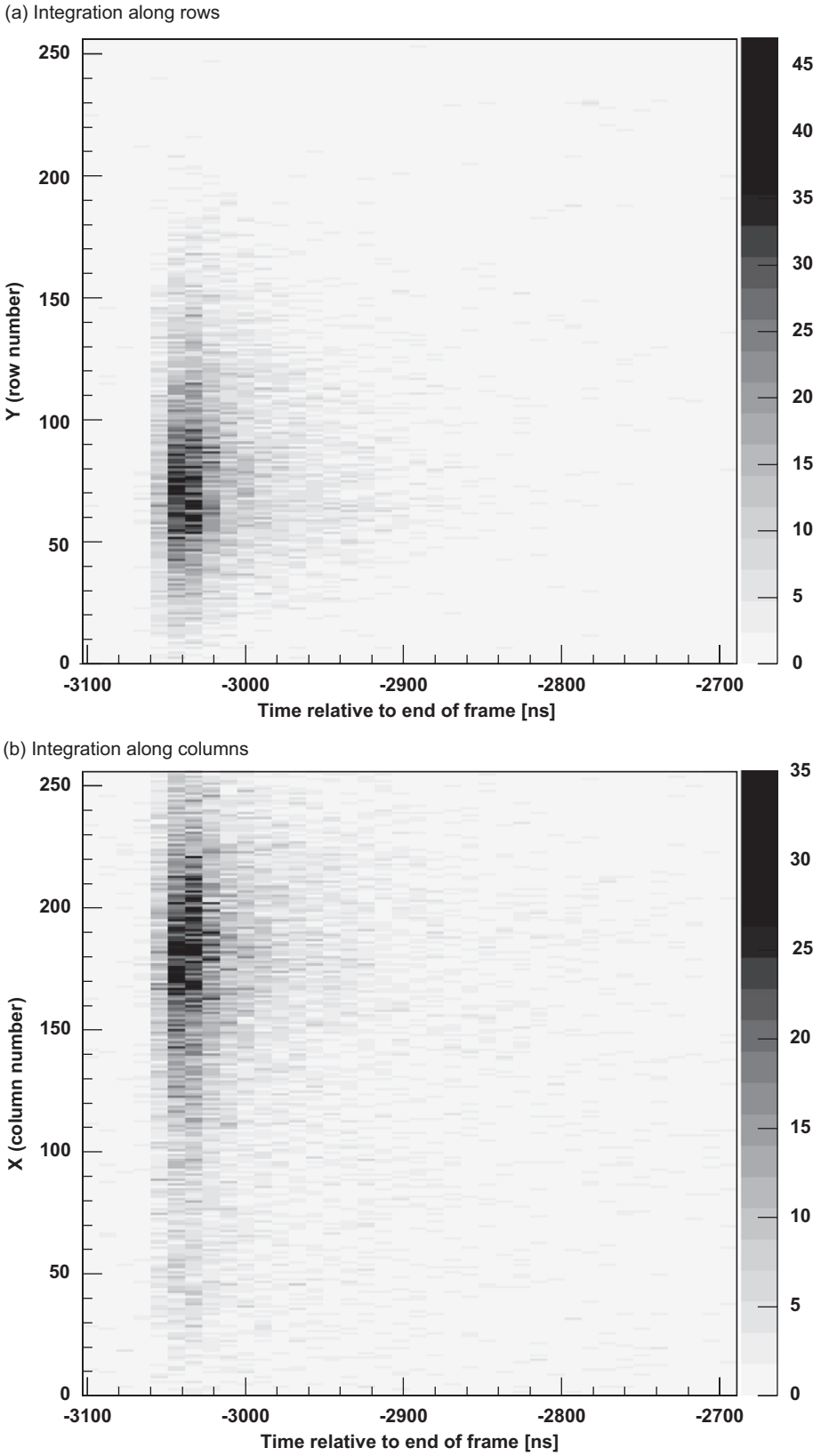

Fig. 4. Image plots of the lamp peak data integrated (a) along rows and (b) along columns.

We show two curves in the plot to better illustrate the effect of charge-sharing among neighboring pixels. In the upper curve also such events are included where the photo-electron actually hits an adjacent pixel but part of its energy is transferred to the central pixel of the 3×3 region. For the lower curve shaded in gray, however, only such events were considered where the photo-

electron directly impinges on the central pixel of the 3 × 3 region. Note that the two curves coalesce for energy depositions above 10 keV since the maximum energy transfer due to charge-sharing is half of the primary energy. This corresponds to the situation when an electron exactly hits the boundary between two pixels.

In our experiments the detector was operated with a discriminator threshold of 4.7 keV in order to maximize the detection efficiency. Due to this relatively low threshold energy hits in the vicinity of pixel boundaries more likely cause multiple pixels to be triggered. The following section will show how this inevitably affects the time resolution.

4.3. Comparison of experiment and simulation

We combine the simulated energy response function from Section 4.2 with a model for the shape of the preamplifier output pulse in the pixel electronics that is motivated by the experiments described in Section 3.2. This serves as an explanation of the long tail in the time distributions shown in Figs. 3a–c.

As pointed out earlier, the pixel electronics shows a time-walk effect, i.e., the time when the charge pulse exceeds the discriminator threshold depends on the energy deposition. We extracted this time-walk from data for several photo-electron energies between 6 and 20 keV using a linear fit as shown in Fig. 6. The peaking time of the preamplifier output pulse amounts to 130 ns as obtained from the slope of the linear fit, which is in agreement with the design parameters of the Timepix pixel cell [9,10].

We used a Fermi-like step function to model the rising edge. The slope of the step function in the linear regime was set equal to the result of the fit in Fig. 6. Different energy depositions are described by rescaling the model pulse without any changes to its shape.

Using this model we have converted the simulated energy response function of Fig. 5 into the detector response in the time domain yielding the result shown in Fig. 7 (top plot). The long tail towards later detection times is primarily due to charge-sharing

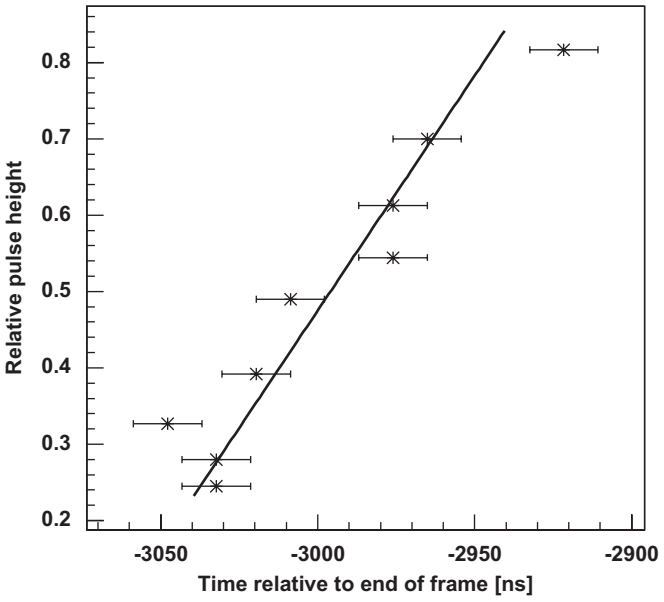

Fig. 6. Rising edge of the preamplifier output pulse as extracted from the peak positions in the experimental data. The relative pulse height is obtained by dividing the discriminator threshold energy of 4.7 keV by the respective photo-electron energy.

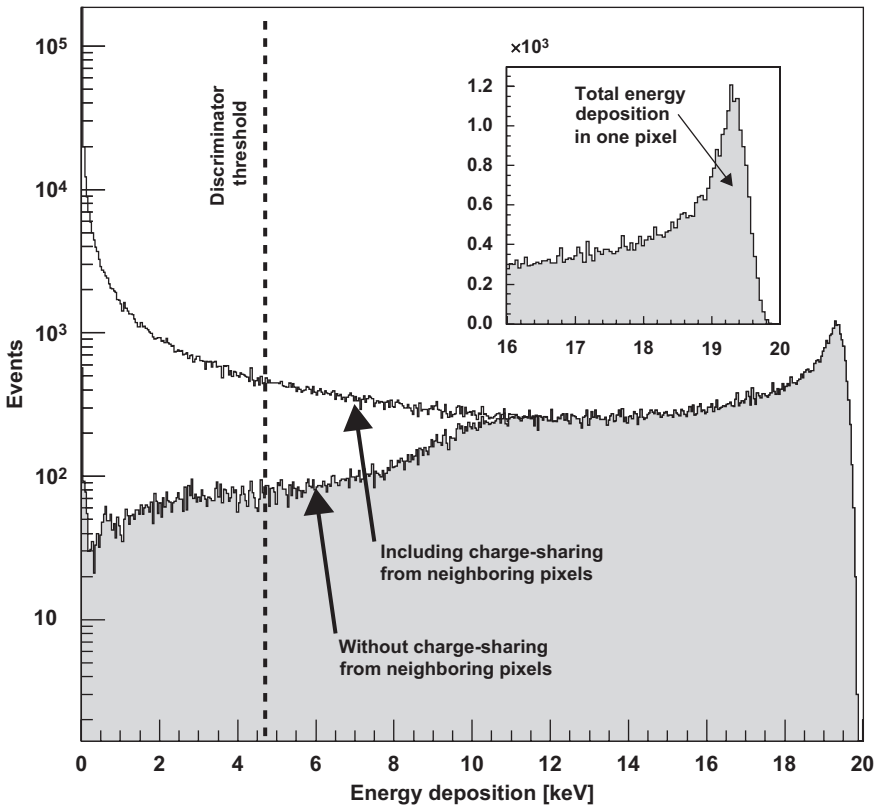

Fig. 5. Simulated energy response function of a pixel on logarithmic scale for a primary energy of 20 keV and 10^5 events per pixel in a 3 × 3 region. Charge-sharing from photo-electrons hitting adjacent pixels are included in the upper curve but left out in the lower curve shaded in gray. The two curves coalesce for energy depositions larger than half of the primary energy. The inset shows on linear scale the peak corresponding to the total energy deposition in one pixel.

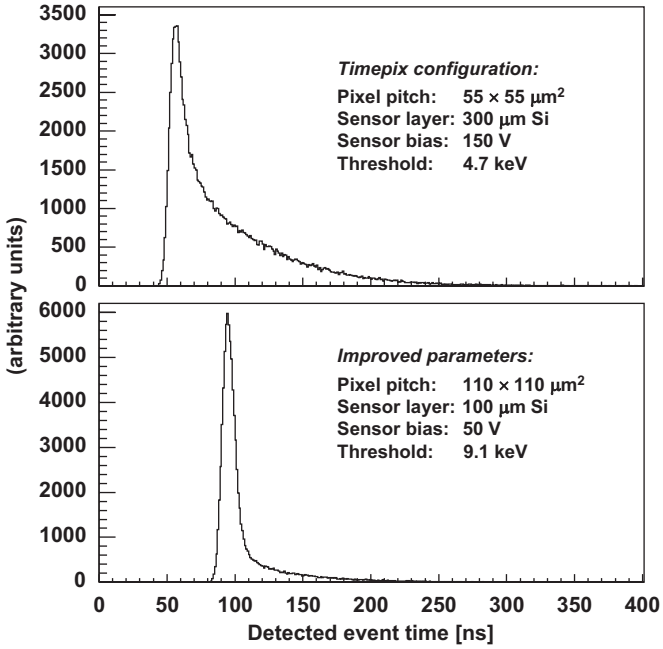

Fig. 7. Detector response in the time domain for the Timepix configuration used in the experiments (top plot) and a set-up with improved parameters (bottom plot). Both simulations use the same Fermi-like step-function derived from Fig. 6 to model the rising edge of the preamplifier output pulse. The response peak for the improved parameters can be fitted with a Gaussian of 4 ns width (sigma).

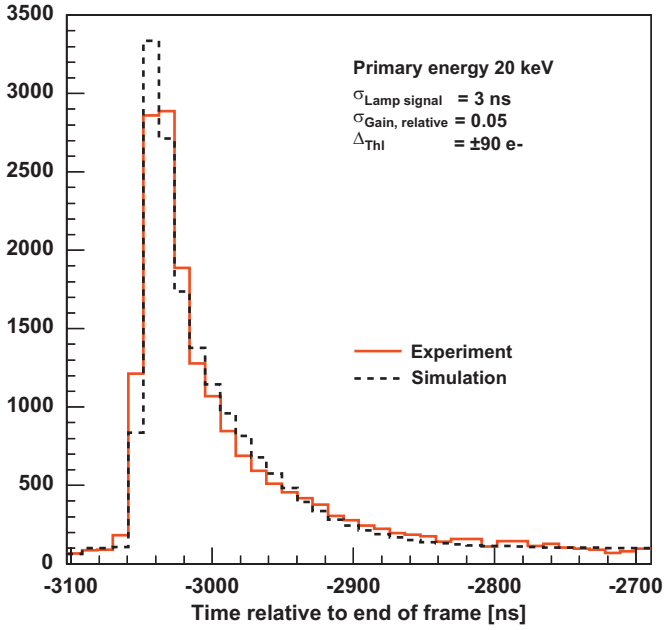

Fig. 8. (Color online) Comparison between the experimental data for 20 keV (solid curve) and the simulation (dashed curve).

among neighboring pixels as can be seen by comparison with the bottom plot of Fig. 7 showing the same plot for larger pixels, a reduced sensor thickness, and a higher discriminator threshold.

The simulation can be compared to the experiment by taking into account an uncertainty of 3 ns of the lamp signal used for the zero point of the time axis, a relative gain variation among the pixels of 5% (Gaussian distribution), and a threshold variation of ±90 electrons (flat distribution). The result is shown in Fig. 8. Very good agreement between experiment and simulation is observed supporting our earlier hypothesis that electron backscattering and charge-sharing among neighboring pixels along with the finite rise time of the preamplifier output pulse limit the time resolution of the photo-electron detection with the Timepix detector.

The main uncertainties in our model are the shape and duration of the rising edge of the preamplifier output pulse. A deviation of the peaking time by ±5 ns has a negligible effect on the agreement between simulation and experiment. The precise shape of the charge pulse would need to be known to further enhance the fit to the data in the region of the tail. Finally, gain and threshold variations were estimated, but only cause a small additional broadening of the signal.

5. Conclusions and outlook

In our experiments we have successfully demonstrated the operation of the Timepix detector in an HPD test set-up. Photo-electrons of energies between 6 and 20 keV were detected. Without the time-walk due to charge-sharing among neighboring pixels, i.e., when considering only single-pixel clusters, a time-resolution of 10.5 ns was measured which agrees well with the detector clock frequency of 100 MHz.

For use in an HPD the easiest way to improve the time resolution is increasing the energy threshold to just below half of the photo-electron energy thereby suppressing backscattering and charge-sharing to a higher degree. This measure, however, will entail a moderate reduction of the detection efficiency. We are going to study it in our next set of experiments. As to the chip design, one would benefit from larger pixels, e.g., 110 μm, and a shorter rise time of the preamplifier output pulse.

The improvement of the time resolution by using larger pixels, a reduced sensor thickness, and a higher discriminator threshold is evident from Fig. 7 and will be investigated in more detail in future simulations.

Acknowledgments

The authors are indebted to Michael Campbell and Xavier Llopart Cudié for the development of the Timepix and would also like to thank the whole Medipix collaboration for further developments and stimulating discussions. T.K.R. was supported by the Studienstiftung des deutschen Volkes.

References

[1] V. Kuntermann, et al., Phys. Rev. B 77 (2008) 115343.
[2] W. Mohler, et al., Methods 29 (2003) 97.
[3] M. Weitz, et al., Phys. Rev. A 52 (1995) 2664.
[4] G. Anton, et al., Nucl. Phys. B Proc. Suppl. 143 (2005) 351.
[5] U.F. Katz, Nucl. Instr. and Meth. A 567 (2006) 457.
[6] The IceCube Collaboration Website: ⟨http://www.icecube.wisc.edu⟩.
[7] M. Alemi, et al., Nucl. Instr. and Meth. A 449 (2000) 48.
[8] T. Gys, Nucl. Instr. and Meth. A 465 (2001) 240.
[9] X. Llopart, et al., Nucl. Instr. and Meth. A 581 (2007) 485.
[10] X. Llopart Cudié, Ph.D. Thesis, Mid Sweden University, 2007.
[11] The Medipix Collaboration Website: ⟨http://www.cern.ch/medipix⟩.
[12] G. Anton, T. Michel, Patent application PCT/EP 2007/005 072.
[13] X. Llopart, et al., IEEE Trans. Nucl. Sci. NS-49 (2002) 2279.
[14] W. Dulinski, et al., Nucl. Instr. and Meth. A 546 (2005) 274.
[15] D.S.S. Bello, et al., Nucl. Instr. and Meth. A 509 (2003) 164.
[16] T. Holy, et al., Nucl. Instr. and Meth. A 563 (2006) 254.
[17] E.H. Darlington, J. Phys. D Appl. Phys. 8 (1975) 85.
[18] A. Korn, et al., Nucl. Instr. and Meth. A 576 (2007) 239.
[19] B. Kreisler, et al., IEEE Nuclear Science Symposium Conference Record, M13-373, 2007.
[20] S. Agostinelli, et al., Nucl. Instr. and Meth. A 506 (2003) 250.
[21] J. Allison, et al., IEEE Trans. Nucl. Sci. NS-53 (2006) 270.
[22] J. Apostolakis, et al., INFN/AE-99/18, Frascati, 1999.
[23] H.G. Spieler, E.E. Haller, IEEE Trans. Nucl. Sci. NS-32 (1985) 419.